FEA of electromagnetic forming using a new coupling algorithm: effects of strain hardening properties and anisotropy

Ali M. Abdelhafeez, M.M. Nemat-Alla, M.G. El-Sebaie

Abstract—Electromagnetic forming is a sheet metal forming technique which utilizes magnetic fields to drive the workpiece deformation at high speed. Modeling of such dynamic deformation is considered as a multi-physics simulation which involves electromagnetic model and mechanical model and a coupling algorithm.

Material properties namely; anisotropy, strain hardening exponent and rate sensitivity index are key factor in controlling such dynamic deformation. A necessity exists for a better understanding of deformation behavior upon variation of such material properties in order to control quality of the deformed product.

In the current investigation, effects of anisotropy, strain hardening exponent and rate sensitivity index on deformation characteristics were studied via FE simulation. An enhanced loose coupling algorithm was proposed by the author in a previous research work and it was utilized in the current research. The simulation results showed that bulge height were inversely proportional to anisotropy value and rate sensitivity and proportional to strain hardening exponent. However, response of thickness and thickness uniformity were opposed to response of bulge height.

Index Terms— Electromagnetic forming, Sheet metal forming, FEM, Enhanced loose coupling, High strain rates, Anisotropy, Work hardening.

1 INTRODUCTION

Electromagnetic forming is one of the high speed forming methods which depends on producing a repulsion electromagnetic pressure between a forming coil and the workpiece using a high pulsed electric current running through the coil.

In the FE simulation of such process two physical models are involved; electromagnetic model and mechanical model. In addition a method of coupling these models is needed. Two coupling methods were used; strong coupling which takes long simulation time and loose coupling which gives inaccurate results.

Loose coupling depends on calculation of the magnetic pressure at beginning of the FE simulation from the electromagnetic model. Then this magnetic pressure entered to the mechanical model which calculates deformation of workpiece. This coupling method ignores the effects of workpiece deformation on magnetic pressure and thus its simulation results have low accuracy. On the other hand, strong coupling hinges on calculation of the magnetic pressure in every simulation time step and then estimation of the corresponding workpiece deformation. Obviously, strong coupling technique gives accurate FE simulation results but it has long duration.

- *Ali M. Abdelhafeez: Mechanical Engineering Dept., Assiut University, Egypt. Email: ali.hassan@eng.au.edu.eg*
- *M. M. Nemat-Alla: Mechanical Engineering Dept., Kafrelsheikh University, Egypt.*
- M. G. El-Sebaie: *Mechanical Engineering Dept., Assiut University, Egypt.*

Good amount of research had been done on EM forming and few were focused on sheet metals bulging. One of the initial researches on sheet metal bulging was made by Takatsu et al. [1]. In which modeling and experimental verifications were made. These experimental data had been used extensively afterwards by other researchers to verify numerical simulations of electromagnetic bulging of sheet metals.

Correia et al. [2] was one of the researchers to simulated Takatsu et al. [1] experimental work using ABAQUS/Explicit software package. Strong coupling was used and rate dependent power law was considered for describing constitutive behavior of the disk material. The results were in modest agreement with previous experimental results of Takatsu et al. [1].

Siddiqui et al. [3] enhanced Correia et al. [2] electromagnetic model. A good agreement with experimental data was noticed. Mesh size was concluded to have negligible influence on results due to small thickness size of workpiece.

Psyk et al. [4] indicated that one of the main problems in FE simulation of EM forming is the long calculation time which attributed to the necessity of meshing not only the workpiece and the tool coil but also the surrounding air. In addition, a very fine mesh of workpiece and coil is needed for getting accurate magnetic field distribution.

A trial to modify the loose coupling method was revealed by Hashimoto et al. [5]. In which, a small portion of the pressure temporal function that corresponds to the first wave of coil current was used. However the FE simulation results showed moderate agreement with experimental data.

Based on Hashimoto [5] trial, Abdelhafeez et al. [6] proposed a modification to the loose coupling technique by considering

International Journal of Scientific & Engineering Research Volume 5, Issue 12, December-2014
ISSN 2229-5518

two waves of the electric current to affect workpiece deformation. Therefore a small part of the magnetic pressure function was considered in the FE simulation. The results showed better agreement with experiment than Hashimoto [5] pressure model.

Another modeling trial was made by L'Eplattenier et al. [7] where a Finite Element Method for the conductors was proposed to couple with Boundary Element Method for the surrounding air/insulators. Unlike FEM, the BEM evade remeshing and infinite boundary problems. However, simulation time was long as BEM generates full dense matrices which require high memory as well as longer CPU calculation time.

Therefore, an unfulfilled necessity for a new coupling method that is fast and accurate exists. A new coupling method which depends on loose coupling technique and accounts for pressure change with workpiece deformation was introduced by Abdelhafeez et al. [8] and is outlined here for completeness.

In the present research, effects of variation of anisotropy, strain hardening exponent and strain rate index was studied numerically using the new coupling method.

2 FINITE ELEMENT SIMULATION

2.1 The New Coupling Method

An EM forming system can be electrically modeled by two magnetically coupled circuits. One circuit represents the capacitor banks, and inductor coil connected in series. The other circuit represents the workpiece.

The mathematical model of the coupled circuits is:

$$(L_1 + L_2).\frac{dI(t)}{dt} + (R_1 + R_2).I(t) + \frac{1}{C}\int I(t)\,dt = 0 \qquad (1)$$

With initial conditions $V=V_0$, $I=0$. Where L_1, L_2 are the inductances of coil and workpiece respectively; R_1, R_2 are the resistances of coil and workpiece respectively; C is the capacitance of capacitor banks; M is the mutual inductance between the two circuits; and $I(t)$ are the electric currents in coil. The solution of this equation is given by [9]

$$I(t) = \frac{V_0}{\omega.(L_1 + L_2)}\, e^{-\beta t} \sin \omega t \qquad (2)$$

Where; $\beta = \frac{(R_1 + R_2)}{2(L_1 + L_2)}$ and $\omega = \sqrt{\frac{1}{(L_1 + L_2).C} - \beta^2}$

The current $I(t)$ is the coil current which generates magnetic field with temporal density $B(t)$. Temporal magnetic field density depends on coil current and geometry and is given by (3).

$$B(t) = \frac{\mu_0 n}{l} I(t) \qquad (3)$$

Where μ_0 is permeability of air and equals $4\pi\times10^{-7}$ H/m; n is number of coil turns; and l is the difference between outer coil radius and inner radius. The magnetic field of the coil current induces eddy currents in the workpiece. The later generate another opposite magnetic field that repels the magnetic field of the coil. The repulsive pressure on the workpiece can be approximated by [10]:

$$p(t) = \frac{B^2(t)}{\mu_0} \qquad (4)$$

Equation (4) represents the temporal behavior of magnetic pressure. On the other hand the pressure distribution on the workpiece is not uniform and depends on the coil geometry. This spatial distribution of the pressure can be only obtained with enough accuracy using FE simulation.

Previous attempts to describe the pressure general function, in the loose coupling method, were considered before by Kleiner et al. [11] to be a multiplicative model as listed in (5).

$$P(r,t) = f(r)\ p(t) \qquad (5)$$

Where $f(r)$ represents pressure spatial distribution over workpiece, and $p(t)$ is the temporal behavior of the pressure. Description of the pressure general function by (5) ignores pressure variation with workpiece deformation which leads to overestimation of FE simulation results. On the other hand, the proposed enhanced loose coupling technique accounts for pressure variation with deformation by considering a deflection dependency function $\varphi(\delta)$ in the pressure general function as expressed by (6).

$$P(r,\delta,t) = p(t)\, f(r)\, \phi(\delta) \qquad (6)$$

The deflection dependency function relates magnetic pressure value with workpiece deflection. The new enhanced loose coupling scheme depends on deflection dependency function that correlates the pressure with deflection of workpiece. Steps of enhanced loose coupling are shown in fig. (1). It is clear that once P(r,δ,t) are known, the mechanical FE simulation can be accomplished. Calculations of deflection dependency function and spatial distribution of magnetic pressure require numerical FE simulations. Details of such FE simulation was presented by the author in previous work [8] and only key findings are depicted in the followings.

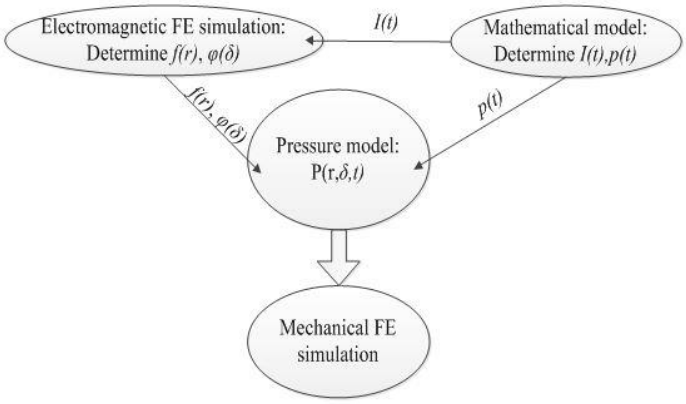

Fig. (1) Schematic diagram of enhanced loose coupling.

Flux density in the gap between coil and workpiece was ob-

International Journal of Scientific & Engineering Research Volume 5, Issue 12, December-2014
ISSN 2229-5518

tained using FEMM simulation package [12] at maximum current value. Magnetic pressure distribution on the workpiece can be estimated from flux density, B, in the gap between coil and workpiece by (7) [13].

$$P(r) = \frac{B(r)^2}{2\mu_o} \tag{7}$$

The pressure distribution over blank radius is shown in fig. (2). This distribution can be approximated using piecewise linear function which represents the spatial distribution function, $f(r)$.

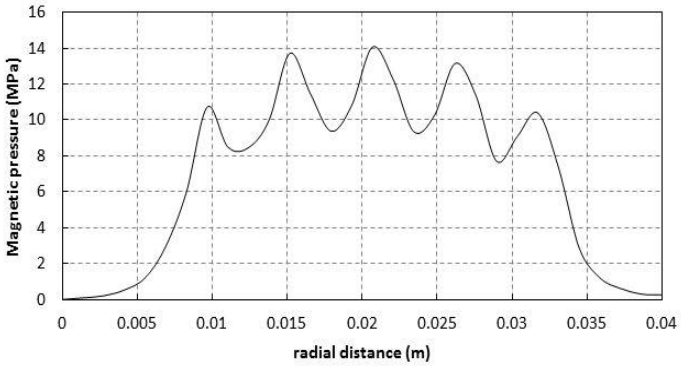

Fig. (2) Magnetic pressure spatial distribution on the workpiece surface at 16 µs.

In order to determine the deflection dependency function $\varphi(\delta)$, gap width was increased and for each new distance, value of corresponding total magnetic force on workpiece was obtained from simulation. Since magnetic pressure is proportional to the total magnetic force, it is a reasonable assumption to consider the normalized total magnetic force equals the normalized pressure. Using least squares curve fitting, these data are fitted by (8) which represents the deflection dependency function, $\varphi(\delta)$.

$$\phi(\overline{\delta}) = 1.24\ \overline{\delta}^{\,-0.824} \tag{8}$$

2.2 Mechanical FE Model

ABAQUS/Explicit 6.12 was adopted for this simulation study. The sheet is considered as a deformable 3D shell part with identical dimensions and properties to the disk of Takatsu et al. [1]. It is meshed with a quadrilateral finite-membrane-strain element with reduced integration which named S4R element. Figure (3) shows meshing of the blank. The mesh consists of 4239 elements with approximate size of 1 mm.
Only the deformable region of the sheet was modeled with diameter of 80 mm. The sheet outer circumference was set to have zero degrees of freedom in the FEM model. The generated heat effect can be neglected in agreement with Kleiner et al. [11], and Conraux et al [14].

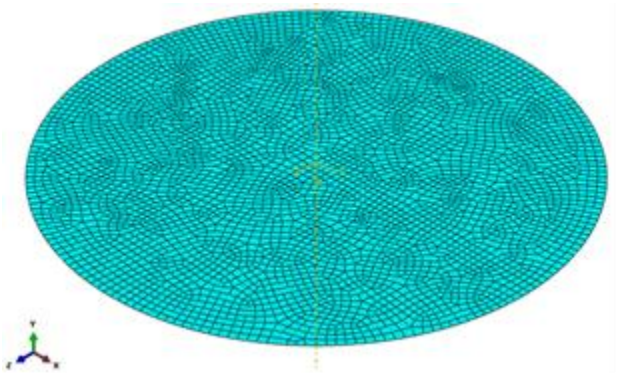

Fig. (3) Un-deformed mesh of the blank.

The load applied on the sheet is pressure with spatial and temporal distribution known as mentioned before. Equations of pressure variation with time, space and workpiece deformation was inputted to ABAQUS/Explicit 6.12 package via user subroutine VDLOAD.
Many strain hardening models extensively used in modeling hardening behavior of JIS A1050-O at high strain rates. According to Abdelhafeez et al. [6], the power law presented in (9) describes the plastic flow of the workpiece material with reasonable accuracy.

$$\overline{\sigma} = 201\ \overline{\varepsilon}^{\,0.27}\,\overline{\dot{\varepsilon}}^{\,0.075}\quad MPa \tag{9}$$

The final deformed workpiece is shown in fig. (4) and a comparison with experimental data of Takatsu [1] deformed disk is depicted in fig. (5).
The proposed enhanced loose coupling scheme was found to be capable of predicting final deformed workpiece shape with reasonable accuracy at low computational cost. Based on this, the model was used for further investigations on anisotropy and strain hardening effects on deformation behavior.

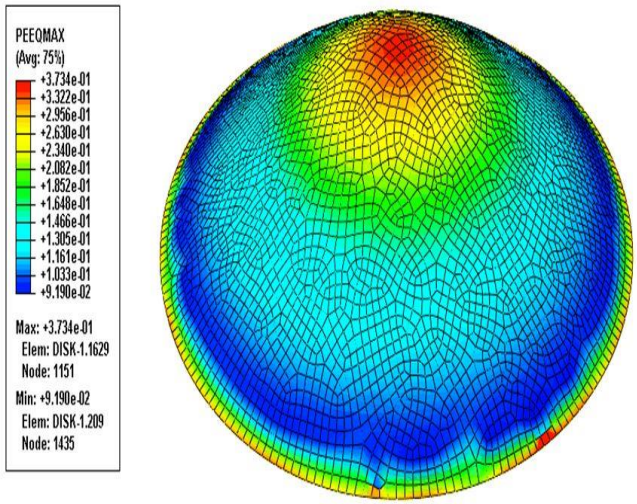

Fig. (4) Effective strain distribution on deformed mesh of the workpiece.

International Journal of Scientific & Engineering Research Volume 5, Issue 12, December-2014
ISSN 2229-5518

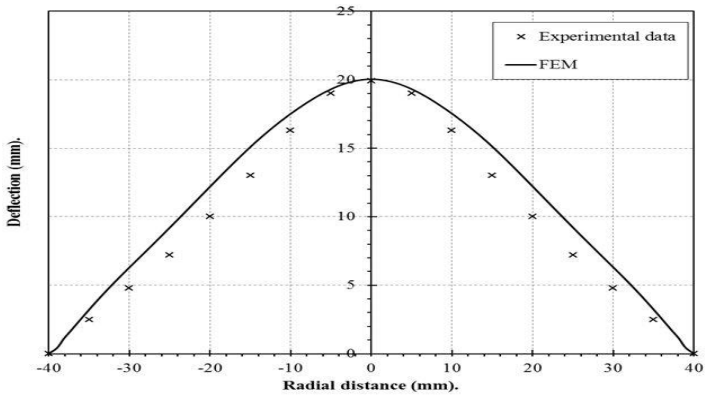

Fig. (5) Workpiece deformation using the new loose coupling contrasted to experimental results of Takatsu et al. [1].

The general form of rate dependent power law is given by

$$\bar{\sigma} = K\,\bar{\varepsilon}^{n}\,\dot{\bar{\varepsilon}}^{m} \tag{10}$$

Where *K* is the strength coefficient, *n* is the hardening exponent, and *m* is the rate sensitivity index. Influence of such factors on deformation characteristics will be studied using the proposed coupling algorithm via FE model.

Another important factor that affects thinning of sheet metals at deformation process is the average anisotropy R-value or Lankford's coefficient. Anisotropy R-value is defined as the ratio of lateral strain to thickness strain of a tension test specimen cut from a sheet metal.

This tension test specimen may be cut in different directions and R-value may be different for each direction. But generally the average R-value is determined by (11).

$$\bar{R} = \frac{R_0 + 2R_{45} + R_{90}}{4} \tag{11}$$

WhereR_0, R_{45}, R_{90} are anisotropy values in direction of rolling, direction inclined by 45^0 on rolling direction, and transverse to rolling direction respectively.

Assuming rotational symmetry about z axis (z axis is the workpiece symmetric axis which is normal to the sheet surface), thus $R_0 = R_{45} = R_{90} = R$ and thus $\bar{R} = R$. This case is known as transverse anisotropy.

Defining anisotropy in ABAQUS is done via the yield stress ratios in x, y, z directions and shear yield stress ratios in xy, yz, zx planes [15]. These ratios are defined by (12)

$$S_{ii} = \frac{\sigma_{ii}}{Y}, S_{ij} = \sqrt{3}\frac{\tau_{ij}}{Y} \tag{12}$$

Where *Y* is a reference yield stress and σ_{ii} is the normal yield stress in *i*-direction and τ_{ij} is the shear yield stress in *ij*-plane. In sheet metal forming applications plane stress condition is generally assumed. Taking reference yield stress equals σ_{11} and using Hill's yield criterion and flow rules give the relations between these ratios and *R* as [16]:

$$S_{11} = S_{22} = 1,\ S_{33} = \sqrt{\frac{\bar{R}+1}{2}},\ S_{12} = \sqrt{\frac{3\bar{R}+3}{4\bar{R}+2}},\ S_{23} = S_{13} = 1 \tag{13}$$

Parameters of workpiece and coil were maintained constant in the simulation runs. The constant parameters are listed in table (1).

Table (1) Input data to the FE model

Coil	
Major radius	32 mm
Number of turns	5
Pitch	5.5 mm
Winding wire diameter	2 mm
Electric conductivity	58 MS/m
Workpiece	
Deformable diameter	80 mm
Thickness	0.5 mm
Density	2750 kg/m^3
Electric conductivity	34.4 MS/m
Modulus of Elasticity	80 GPa
Yield stress	22 MPa
Poisson's ratio	0.33
Coil-workpiece gap	1.6 mm
Discharge circuit	
Total inductance	2.86 μH
Total resistance	25.5 mΩ
Total capacitance	40 μF
Charging voltage	6 kV

3 Results and Discussion

3.1 Effects of Anisotropy Variation

Lankford's coefficient (*R*) was selected to have values of 0.5, 0.8, 1.5, 2, and 4. For each R-value, yield stress ratios were calculated according to (13) and entered to the model as listed in table (2). For each R-value a FE simulation was done and results were acquitted.

The strain hardening exponent (*n*), rate sensitivity index (*m*), and strength coefficient (*K*) are selected to be 0.27, 0.075, and 201 MPa respectively.

Table (2) Yield stress ratios for the used R-values

	***R*= 0.5**	**0.8**	**1.5**	**2**	**4**
S_{11}, S_{22}, S_{23}, S_{13}	1	1	1	1	1
S_{33}	0.866	0.949	1.118	1.225	1.581
S_{12}	1.061	1.0191	0.968	0.949	0.913

Deformed workpiece final profiles for each *R* value are shown in fig. (6). From fig. (6) it is obvious that increase in anisotropy value makes the material resistant to bulging or in other words resistant to section thinning. Maximum deflection values are 21.8, 20.6, 18.7, 17.7, and 15.3 for R-values of 0.5, 0.8, 1.5, 2, and 4 respectively. No change in profile shape was noticed and the change only is in the size of the profile and this prove that final profile of workpiece is dependent on pressure temporal and spatial distribution only.

Figure (7) illustrates blank thickness variation along its radius for each R-value. It is clear that thickness of blank generally increases while moving outwards from center of the blank.

International Journal of Scientific & Engineering Research Volume 5, Issue 12, December-2014
ISSN 2229-5518

Localized thinning at outer regions was also noticed which can be explained as a reason of excessive bending at these regions.

Thickness average values are 0.398, 0.408, 0.425, 0.433, and 0.452 for R-values of 0.5, 0.8, 1.5, 2, and 4 respectively, i.e. average thickness increase with increasing R-value. Blank thickness dispersion can be estimated by the standard deviation. Standard deviation is a widely used measure of variability or diversity used in statistics and probability theory. It shows how much variation or dispersion exists from the average. A low standard deviation indicates that the data points tend to be very close to the mean, whereas high standard deviation indicates that the data points are spread out over a large range of values. Standard deviation of thickness values are 0.046, 0.039, 0.028, 0.0235, and 0.014 for R-values of 0.5, 0.8, 1.5, 2, and 4 respectively which mean that thickness of blank tend to be more uniform along radius with increasing of R-value.

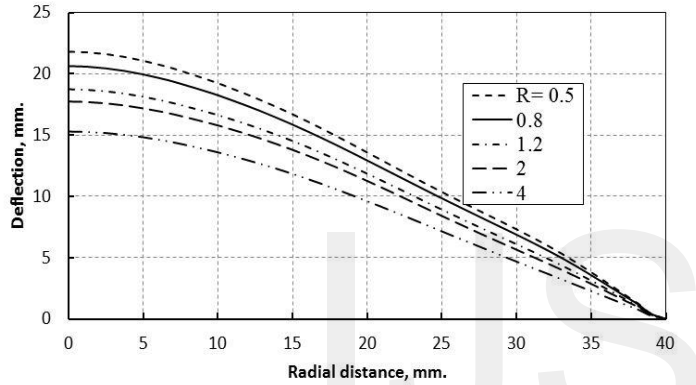

Fig. (6) Workpiece final profile at end of deformation for different R-value.

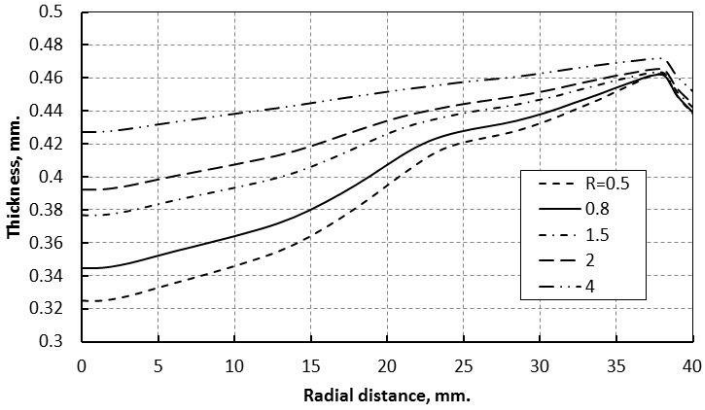

Fig. (7) Blank thickness variation over radius for different R-values.

3.2 Effects of Strain Hardening Exponent

Values of strain hardening exponent (*n*) for most metals are ranging from 0.1 to 0.5 at normal conditions [17]. Thus n-values were selected to be 0.1, 0.2, 0.3, 0.4, and 0.5. *R*-value was set to value of 1 which represents isotropic material. Rate sensitivity index (*m)* and strength coefficient (*K*) were adopted to be 0.075, and 201 MPa respectively. Workpiece and coil properties are all as mentioned before in table (4.1). Our new FE model was used for simulation with each n value and the results was obtained.

Figure (8) represents the final profile of deformed blank for various n-values. Maximum deflection occurs at center with values of 25.3, 23.1, 20.7, 18.4, and 15.6 for *n* value of 0.5, 0.4, 0.3, 0.2, and 0.1 respectively. By increasing *n*, the material becomes softer (i.e. it get large strain with small stress applied on it) and hence its deflection increase as noticed from figure. It is clear from figure that *n* has no effect on deformed workpiece shape and change is only in size of deformation.

Figure (9) illustrates thickness variation over blank radius for various n values. Maximum thinning occurs at center with values of 0.39, 0.37, 0.35, 0.33, and 0.31 for *n* values of 0.5, 0.4, 0.3, 0.2, and 0.1 respectively. Thinning decrease gradually with moving away from blank center toward perimeter and then it is locally increases at outer boundaries because of excessive bending at this area. Average thicknesses are 0.44, 0.42, 0.41, 0.39, and 0.38 for *n* values of 0.1, 0.2, 0.3, 0.4, and 0.5 respectively. Thus increasing *n* value reduces the average thickness of the sheet. Standard deviations of thickness variation are 0.031, 0.034, 0.036, 0.038, and 0.039 for *n* values of 0.1, 0.2, 0.3, 0.4, and 0.5 respectively which mean that *n* value has a very small effect on final blank thickness uniformity.

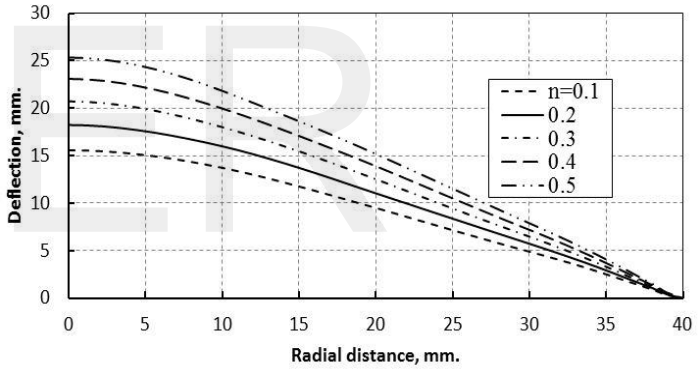

Fig. (8) Workpiece final profile at end of deformation for different n-value.

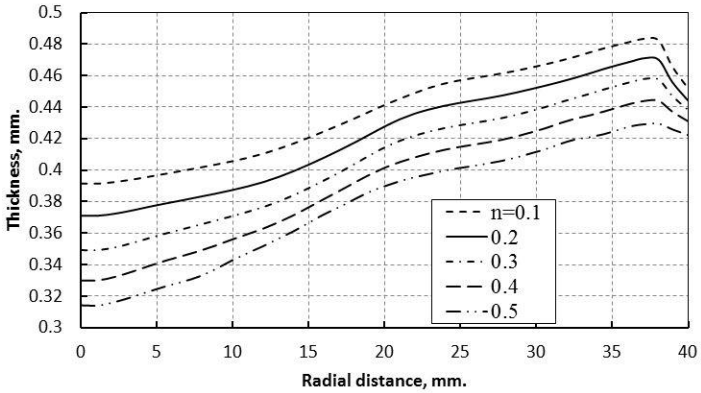

Fig. (9) Blank thickness variation along its radius for different n-values.

International Journal of Scientific & Engineering Research Volume 5, Issue 12, December-2014
ISSN 2229-5518

3.3 Effects of Rate Sensitivity Index

Rate sensitivity index *m* for most metals are less than 0.1 at homologous temperature less than 0.7 [18]. Values of *m* were selected to be 0.01, 0.03, 0.05, 0.07, and 0.1. Values of *R*, *n*, and *K* are set to be 1, 0.27, and 201 MPa respectively. Workpiece and coil properties are all as mentioned before in table (1). Our new FE model was used for simulation with each n value and the results was obtained.

Figure (10) represents the final profile of deformed blank for various m-values. Maximum deflection occurs at center with values of 26.3, 24.1, 22.2, 20.4, and 18.1 for *m* values of 0.01, 0.03, 0.05, 0.07, and 0.1 respectively. By increasing *m*, the material becomes stiffer (i.e. it get small strain with large stress applied on it) and hence its deflection decrease as noticed from figure. It is clear from figure that *m* has no effect on deformed workpiece shape and change is only in size of deformation.

Figure (11) illustrates thickness variation over blank radius for various *m* values. Maximum thinning occurs at center with values of 0.296, 0.313, 0.331, 0.351, and 0.378 for *m* values of 0.01, 0.03, 0.05, 0.07, and 0.1 respectively. Thinning decrease gradually with moving away from blank center toward perimeter and then it is locally increases at outer boundaries because of excessive bending at this area. Average thicknesses are 0.372, 0.385, 0.398, 0.41, and 0.425 for *m* values of 0.01, 0.03, 0.05, 0.07, and 0.1 respectively. Thus increasing *m* value increase the average thickness of the sheet. Standard deviations of thickness variation are 0.049, 0.046, 0.042, 0.037, and 0.030 for *m* values of 0.01, 0.03, 0.05, 0.07, and 0.1 respectively which mean that increasing *m* value increases final blank thickness uniformity.

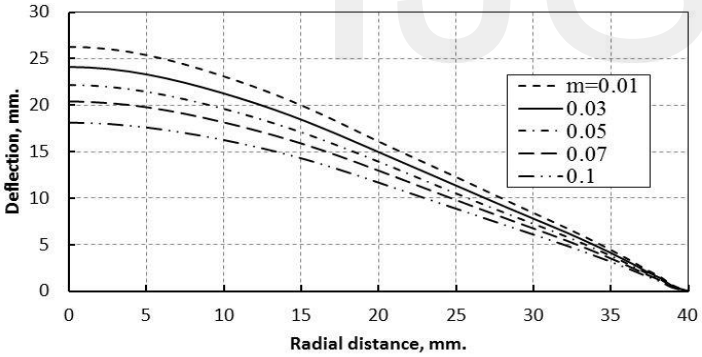

Fig. (10) Workpiece final profile at end of deformation for different m-value.

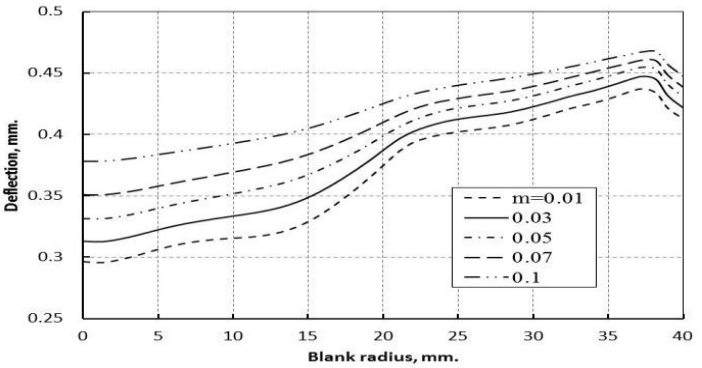

Fig. (11) Thickness variation for different m values.

4 CONCLUSIONS

Changing *R*, *n*, and *m* values on illustrated that average thickness is proportional to *R* and *m* values and inversely proportional to *n* values. Therefore increasing *m*, and *R* value reduces section thinning due to bulging and increasing *n* value enhances section thinning.

On the other hand, the uniformity of workpiece thickness is proportional to *R*, and *m* values while increasing *n* value reduces section uniformity after deformation.

In addition, It was clear that increasing *R*, and *m* values makes the workpiece material more harder and therefore the center deflection decreases. On the other hands increasing n value makes the material softer and thus center deflection increases.

Despite the study is based on verified model, the results can help in controlling thickness variation at such dynamic forming process and would help in industrial applications.

REFERENCES

[1] N. Takatsu, M. Kato, K. Sato and T. Tobe, High Speed Forming Of Metal Sheets By Electromagnetic Force, JSME International Journal, vol. 31, pp. 142–148, 1988.

[2] J.P.M. Correia, M.A. Siddiqui, S. Ahzi, S. Belouettar and R. Davies, A Simple Model To Simulate Electromagnetic Sheet Free Bulging Process, International Journal of Mechanical Sciences, vol. 50, pp. 1466–1475, 2008.

[3] M.A. Siddiqui, J.P.M. Correia, S. Ahzi and S. Belouettar, A Numerical Model To Simulate Electromagnetic Sheet Metal Forming Process, International Journal of Material Forming, vol. 1, pp. 1387–1390, 2008.

[4] V. Psyk, D. Risch, B.L. Kinsey, A.E. Tekkaya and M. Kleiner, Electromagnetic Forming – A Review, Journal of Material Processing Technology, vol. 211, pp. 787–829, 2011.

[5] Y. Hashimoto, H. Hideki, S.Miki and N. Hideaki, Local Deformation And Buckling Of A Cylindrical Al Tube Under Magnetic Impulsive Pressure, Journal of Material Processing Technology, vol. 85, pp. 209–212, 1999.

[6] A.M. Abdelhafeez, M.M. Nemat-Alla and M.G. El-Sebaie, Finite Element Analysis Of Electromagnetic Bulging Of Sheet Metals, International Journal of Scientific and Engineering Research, vol. 3, 2012.

[7] P. L'Eplattenier, G. Cook and C. Ashcraft, Introduction Of An Electromagnetism Module In LS-DYNA For Coupled Mechanical Thermal Electromagnetic Simulations, 3rd International Conference on High Speed Forming, Dortmund, Germany (2008), 85–96.

[8] A.M. Abdelhafeez, M.M. Nemat-Alla, M.G. El-Sebaie, FEA Of Electromagnetic Forming Using A New Coupling Algorithm, International Journal of Applied Electromagnetics and Mechanics, vol. 42 (2), pp. 157-169, 2013.

[9] G.K. Lal and M.J. Hiller, The Electrodynamics Of Electromagnetic Forming, International Journal of Mechanical Sciences, vol. 10, pp. 491–500, 1968.

[10] F.M. Song, X. Zhang, Z.R.Wang and L.Z. Yu, A Study Of Tube Electromagnetic Forming, Journal of Material Processing Technology, vol. 151, pp. 372–375, 2004.

[11] M. Kleiner, C. Beerwald and W. Homberg, Analysis Of Process Parameters And Forming Mechanisms Within The Electromagnetic Forming Process, CIRP Annals – Manufacturing Technology, vol. 54, pp. 225–228, 2005.

[12] D.C. Meeker, Finite Element Method Magnetics, Version 4.2, (11 Oct 2010 Build), http://www.femm.info/wiki/HomePage

International Journal of Scientific & Engineering Research Volume 5, Issue 12, December-2014
ISSN 2229-5518

[13] A.G. Mamalis, D.E. Manolakos, A.G. Klados and A.K. Koumoutsos, Physical Principles Of Electromagnetic Forming Process: A Constitutive Finite Element Model, Journal of Material Processing Technology, vol. 161 (2005), pp. 294–299.
[14] P. Conraux, M. Pignol, V. Robin and J.M. Bergheau, 3D Finite Element Modeling Of Electromagnetic Forming Processes, 2nd International Conference on High Speed Forming, Dortmund, Germany (2006), 73–83.
[15] ABAQUS Analysis User's Manual: Volume 3, Dassault Systèmes, 2011.
[16] Cheng, P., Yao ,Y.L., The Influence Of Sheet Metal Anisotropy On Laser Forming Process, J. Of Manuf. Sci. And Eng., vol. 127(August), pp. 572-582, 2005.
[17] Groover, M., Principles Of Modern Manufacturing, John Wiley & Sons, 2011.
[18] Hosford, W., Caddell, M., Metal Forming Mechanics and Metallurgy, Cambridge University Press, 2011.